Phase diagram and critical behavior of a forest-fire model in a gradient of immunity

Nara Guisoni,[1,2,*] Ernesto S. Loscar,[1] and Ezequiel V. Albano[2,3]

[1]*Instituto de Investigaciones Fisicoquímicas Teóricas y Aplicadas (INIFTA), Facultad de Ciencias Exactas, Universidad Nacional de La Plata, CONICET CCT-La Plata, Sucursal 4, CC 16 (1900) La Plata, Argentina*

[2]*Instituto de Física de Líquidos y Sistemas Biológicos (IFLYSIB), Universidad Nacional de La Plata, CONICET CCT-La Plata, CC 565 (1900) La Plata, Argentina*

[3]*Departamento de Física, Facultad de Ciencias Exactas, Universidad Nacional de La Plata, La Plata, Argentina*

(Received 26 July 2010; revised manuscript received 12 December 2010; published 25 January 2011; publisher error corrected 1 February 2011)

The forest-fire model with immune trees (FFMIT) is a cellular automaton early proposed by Drossel and Schwabl [Physica A **199**, 183 (1993)], in which each site of a lattice can be in three possible states: occupied by a tree, empty, or occupied by a burning tree (fire). The trees grow at empty sites with probability p, healthy trees catch fire from adjacent burning trees with probability $(1-g)$, where g is the immunity, and a burning tree becomes an empty site spontaneously. In this paper we study the FFMIT by means of the recently proposed gradient method (GM), considering the immunity as a uniform gradient along the horizontal axis of the lattice. The GM allows the simultaneous treatment of both the active and the inactive phases of the model in the same simulation. In this way, the study of a single-valued interface gives the critical point of the active-absorbing transition, whereas the study of a multivalued interface brings the percolation threshold into the active phase. Therefore we present a complete phase diagram for the FFMIT, for all range of p, where, besides the usual active-absorbing transition of the model, we locate a transition between the active percolating and the active nonpercolating phases. The average location and the width of both interfaces, as well as the absorbing and percolating cluster densities, obey a scaling behavior that is governed by the exponent $\alpha = 1/(1+\nu)$, where ν is the suitable correlation length exponent ($\nu_\perp$ for the directed percolation transition and ν for the standard percolation transition). We also show that the GM allows us to calculate the critical exponents associated with both the order parameter of the absorbing transition and the number of particles in the multivalued interface. Besides, we show that by using the gradient method, the collapse in a single curve of cluster densities obtained for samples of different side is a very sensitive method in order to obtain the critical points and the percolation thresholds.

DOI: 10.1103/PhysRevE.83.011125 PACS number(s): 05.70.Fh, 02.50.−r, 64.60.ah, 82.20.Wt

I. INTRODUCTION

A wide class of far-from-equilibrium systems exhibits irreversible phase transitions (IPTs) between an active phase and an inactive (absorbing) regime, so that the system becomes irreversibly trapped into the absorbing phase when a suitable control parameter is finely tuned across the transition point. In fact, IPTs have been reported in models for heterogeneously catalyzed reactions [1], prey-predator systems [2], epidemic propagation [3], as well as in different models proposed to mimic biological systems, such as the immune system [4], the spreading of virus propagation [5], and calcium propagation inside the cells [6–8]. In contrast, self-organized criticality (SOC) describes the way in which some nonequilibrium systems develop power-law correlations in a steady state without any tuning of parameters to a given value. The concept of SOC has attracted much interest since it might explain the spontaneous onset of scale-free distributions in nature, economy, social sciences, etc. [9].

Within this broad context, we focus our attention on a forest-fire model with immune trees, which is a variant of the model early introduced by Bak, Chen, and Tang [10]. In general, forest-fire models are a cellular automaton, so that each site of a d-dimensional hypercubic lattice can be in three different states: occupied by a tree, occupied by a burning tree, or empty. The system is updated in parallel as follows:

(i) A burning tree becomes an empty site.

(ii) A tree grows with probability p at empty sites.

(iii) A green tree becomes a burning tree with probability $1-g$ if at least one of its nearest neighbors is burning.

(iv) A tree becomes a burning tree with probability $f \ll 1$ if no neighbor is burning.

In the original version [10] the forest-fire model was presented with only one control parameter, the tree growth probability p (that is, $f = 0$ and $g = 0$), and shows regular spiral-shaped fire fronts in the limit of $p \to 0$ [11,12]. The most studied version of the model, proposed by Mossner, Drossel, and Schwabl [12], included the nonzero lightning parameter f (with $g = 0$). For this version in the limit $f/p \to 0$, the model has been shown to exhibit SOC in a nonconservative system for the first time. Self-organization is found in the model of Mossner, Drossel, and Schwabl because the steady state is independent of both the initial conditions and the exact values of the parameters, as long as f/p is small enough. The system is critical because there are power-law correlations over long distances and long time intervals [13]. Later, the inclusion of the immunity $g \neq 0$ in the model [14,15] by means of rule (iii) was proposed. When the immunity is considered (with $f = 0$), depending on the value of g, the model exhibits a second-order IPT between an active phase and an absorbing phase, in which all sites are occupied by green trees. This version of the model is known as the forest-fire

*naraguisoni@conicet.gov.ar

model with immune trees (FFMIT) and it is the focus of the present work.

The main features of the phase diagrams of far-from-equilibrium models, such as the FFMIT, can be predicted by means of different analytic approximations, but usually the most accurate tool to obtain this kind of phase diagram is the computational simulation [16]. According to the usual simulation method used in the FFMIT [14,15,17], for a fixed arbitrary value of the tree growth probability p ($0 < p \leqslant 1$) and by starting from the active phase, an increment of g causes the fire density to decrease until the fire becomes irreversibly extinguished at a certain critical point (p, g_c). The set of critical points defines a critical curve $g_c(p)$ that, in the limit of infinite lattice size ($L \to \infty$), divides the phase space into two regions: the active state for $g < g_c(p)$, where fire fronts are present, and the unique absorbing state for $g > g_c(p)$, where all sites are occupied by green trees.

In this paper we study the FFMIT by means of the gradient method (GM) [18], instead of the standard simulation procedure [14,15,17]. In order to apply the GM to the FFMIT, we consider the immunity g as a uniform gradient along the horizontal axis of the lattice. Then, in each simulation, the GM provides an overview of the behavior of the system for the whole range of the immunity, at fixed p, of course, in contrast to the standard simulation method, which requires an individual (independent) simulation for each value of g and p. As will be shown below, by using the GM in the FFMIT, besides the usual second-order IPT, we can also locate a percolation transition of the green trees inside the active phase of the model. We also obtained the critical points and several exponents associated with these transitions.

The GM for the study of IPTs is a generalization of the so-called gradient percolation method [19,20]. The gradient percolation method has been used to study the percolation transition in models where the density is the control parameter [20]. It is worth mentioning that by using the GM, despite the percolation transition, one is also able to study continuous and first-order IPTs. An approach related to the gradient percolation method, widely used in the study of colloids and polymers, is the so-called sedimentation equilibrium method [21]. By measuring concentration profiles of lattice polymers in a gravitationlike potential [21,22], which generates the gradient, the equation of state can be inferred if a local density approximation as in hydrostatic equilibrium is invoked. We organized the paper as follows: in Sec. II we summarize results of the gradient percolation approach and introduce the GM for the case of the FFMIT. Results of Monte Carlo simulations obtained by applying the GM to the FFMIT are presented and discussed in Sec. III. Finally, our conclusions are stated in Sec. IV.

II. THEORETICAL BACKGROUND AND DEFINITIONS OF THE GRADIENT METHOD

A. Gradient percolation

The standard percolation transition was first shown to be related to the diffusion front of noninteracting particles in the seminal work of Sapoval *et al.* [19]. The diffusion of noninteracting particles, except for the excluded volume, produces a concentration gradient along the source-well direction. By considering a different connectivity between particles and holes, one can define an interface that constitutes the *diffusion front*. This interface is multivalued and self-similar, and it can be used in order to measure the properties of the percolation transition. In fact, the diffusion front, for the case of an infinite lattice size, corresponds to the hull of the incipient percolation cluster [19,23]. As the concentration of particles $p(x,t)$ depends on their position, decreasing from the source to the well, one actually has a gradient percolation system. The concentration of particles at the mean front position (x_f) is the same as the percolation threshold p_c, that is, $p(x_f) = p_c$.

Sapoval *et al.* [19] have demonstrated, by using heuristic arguments, that both the width of the diffusion front (W_L) and the number of particles that constitute it (N) scale with the gradient density in the locus of the front $[\nabla p(x_f)]$. That is,

$$W_L \sim [\nabla p(x_f)]^{-\alpha^*} \quad \text{where} \quad \alpha^* = \frac{\nu}{\nu+1}, \tag{1}$$

and

$$\frac{N}{L_y} \sim [\nabla p(x_f)]^{-\alpha^N} \quad \text{where} \quad \alpha^N = \frac{1}{\nu+1}. \tag{2}$$

$\nu = 4/3$ is the critical exponent of the correlation length for the standard percolation transition [24], and L_y is the side of the lattice parallel to the interface (or perpendicular to the gradient direction). Recently, Nolin [25] has proved the results of Eqs. (1) and (2), as predicted by Sapoval, for the case of site percolation in a triangular lattice.

From the point of view of the dynamic scaling theory of self-affine interfaces early developed by Family and Vicsek [26], an interface width W_L should scale according to

$$W_L \sim L_y^{\alpha^*}, \tag{3}$$

where α^* is the roughness exponent and L_y is the finite length along the direction parallel to the interface. For the diffusion front, one could expect that Eq. (3) will be recovered if one considers a linear gradient. However, for the self-similar interface generated by the diffusion of noninteracting particles, the correlations are constrained by the concentration gradient and consequently the scaling behavior is dominated by the growing correlation length along the direction where the gradient is applied, i.e., the direction perpendicular to the interface. In fact, it has been demonstrated [27] that for a linear concentration of particles, the dynamic scaling theory works, but by taking the length perpendicular to the interface L_x since L_y becomes irrelevant. So, for the diffusion front in a constant gradient, the Family-Vicsek scaling behavior [Eq. (3)] should be replaced by

$$W_L \sim L_x^{\alpha^*}. \tag{4}$$

Note that this equation is a particular case of the general relationship given by Eq. (1) when one considers a constant gradient.

The use of the relationships expressed in Eqs. (1) and (2) in the diffusion front problem allowed for the measurement, with very high precision, of both the percolation threshold [28] and the exponent ν [27] for the standard percolation transition. The idea of defining an interface based on the geometrical properties of the diffusion front (actually by using the hull of

the incipient percolation cluster) and calculating the critical concentration of the percolation transition from the location of that interface has been called the *gradient percolation method*. Subsequently, the gradient percolation method has been applied extensibly in different models where the density is the control parameter [20]. In a related context, Kolb *et al.* have applied the gradient percolation method to the study of spinodal decomposition in a lattice gas [29]. A generalization of the results of the gradient percolation method to diffusion front models with radial symmetry was made recently by Nolin [30]. Furthermore, Gabrielli *et al.* have presented a field theory description of a model for dynamical etching showing a rich physical behavior, related to gradient percolation, which involves self-organization and the existence of absorbing states when the etching process is stopped [31].

B. Gradient method

By extending the early ideas of the gradient percolation method, we have recently proposed the so-called *gradient method* (GM) for the study of IPTs of both first and second order, as well as the standard percolation transition. The GM can be applied to a wide variety of irreversible models. The first step necessary for the implementation of the GM is to impose a gradient on one of the control parameters of the model. This condition generates a configuration that forces a gradient concentration. In the case of the FFMIT we impose a constant gradient on the control parameter g (immunity) along the horizontal (x direction) axis, for a fixed given value of p.[1] In this way the immunity is given by

$$g(x) = \frac{x}{L_x}, \tag{5}$$

where L_x is the horizontal lattice side and $1 \leqslant x \leqslant L_x$. For steady states, some relevant properties such as the densities of trees, burning trees, and empty sites depend only on the parameters p and $g(x)$. In Fig. 1(a) we show a typical stationary configuration of the FFMIT with $g(x)$ given by Eq. (5).

In the snapshot of Fig. 1(a) one can see a green cluster that obviously percolates along the vertical direction (right-hand side), and on the left-hand side of the sample one has that the green trees do not percolate anymore. Therefore it is clear that there is a percolative-nonpercolative transition of green trees, which can be studied by analyzing the self-similar interface. In order to find this interface we proceed as follows. One first determines all the green sites in contact with the green cluster, located on the right-hand side of the sample. These sites, connected by means of nearest neighbors, are denoted as the "land." Empty sites and burning trees are linked through both nearest and next-nearest-neighbor sites and form a large cluster that is termed the "sea." The sites that are neither connected with the large clusters of land nor of sea are identified as "islands" and "lakes," respectively, but they are irrelevant. In fact, the interface is given by the seashore where land and sea are in contact [19,27,32]. We call the set of these sites $\{x_j, j = 1, \ldots, N_{\mathrm{MVI}}\}$ the multivalued interface (MVI).

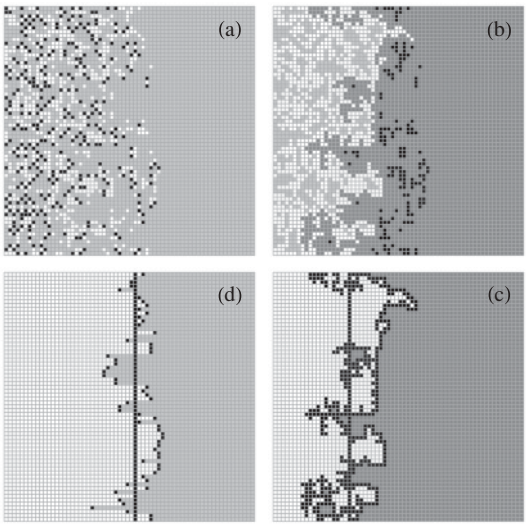

FIG. 1. FFMIT in a linear gradient of immunity for a square lattice of $L = 64$ ($p = 0.5$), after a transient of 500 Monte Carlo steps (MCSs). All figures correspond to the same configuration. (a) Typical snapshot. The burning trees are represented by the black sites, the green trees by the gray sites, and the empty sites are left white. On the left-hand side of the figure we can see the active region, whereas on the right-hand side the system is in the absorbing state, with all sites taken by green trees. (b) Identification of the land (gray sites), the sea (white sites), the islands (light gray sites), and the lakes (black sites). (c) Islands and lakes of (b) were eliminated in order to easily identify the MVI, shown with the black sites. The average position of the MVI is the black vertical line. On the right-hand side of the figure (gray sites) we can see the cluster of percolation particles. (d) The SVI is identified with the black sites and the average position of the SVI is the black vertical line. On the right-hand side of the SVI one has only green trees, defining the absorbing cluster (gray sites). On the left-hand side of the SVI one has the active phase (white sites), with all states represented by the same color for the sake of clarity.

Figure 1(b) shows the land (gray), the sea (white), as well as the islands (light gray) and lakes (black). In order to make the meaning of the MVI clearer, in Fig. 1(c) we dismiss islands and lakes present in Fig. 1(b). The MVI shown in Fig. 1(c) is identified with the seashore (black sites), which is the border between the percolating phase (gray sites) and the nonpercolating phase (white sites), on the right-hand and left-hand sides of the sample, respectively. The mean position of the MVI is the black vertical line.

An interface can be characterized by two observables: its mean position and its width. Of course these observables are measured in terms of the x coordinate, but here for the sake of clarity of the paper it is more convenient to measure these observables in units of the parameter g, just by using Eq. (5). The average immunity undergone by the sites belonging to the MVI ($\{x_j, j = 1, \ldots, N_{\mathrm{MVI}}\}$) is given by

$$g^{\mathrm{MVI}} = \frac{1}{N_{\mathrm{MVI}}} \sum_{j=1}^{N_{\mathrm{MVI}}} g(x_j), \tag{6}$$

[1] We expect exactly the same results if one imposes the gradient on the control parameter p, rather than on the immunity. Namely, Gastner *et al.* [32] have shown that the results for the gradient percolation method applied to the contact process are independent of the control parameter selected to apply the gradient.

and it is identified as the percolation threshold g_p [18], as in the case of the gradient percolation method.

On the other hand, the width of the MVI is given by

$$w^{\mathrm{MVI}} = \sqrt{\frac{1}{N_{\mathrm{MVI}}} \sum_{j=1}^{N_{\mathrm{MVI}}} [g(x_j) - g^{\mathrm{MVI}}]^2}. \tag{7}$$

The previous scaling relationship formulated for the width of the interface in the diffusion front problem [Eq. (4)] is also valid for the MVI defined here. However, it is convenient to rewrite Eq. (4) because in the GM the width is measured in units of g. Therefore one has that $w = (dg/dx)W_L$, where W_L is the width measured in lattice units. Because $g(x) = (x/L_x)$, one obtains $w = (1/L_x)W_L \propto L_x^{\alpha^*-1}$. Then the width scales as

$$w \propto L_x^{-(1-\alpha^*)} = \Delta^{1-\alpha^*}, \tag{8}$$

where Δ is the gradient. Considering that $\alpha^* = \frac{\nu}{\nu+1}$ [from Eq. (1)] and by taking $\alpha = 1 - \alpha^*$, we conclude that the width in the GM scales as [18]

$$w \propto \Delta^{\alpha} \quad \text{where} \quad \alpha = \frac{1}{1+\nu}. \tag{9}$$

For the MVI one should consider $\nu = 4/3$, which corresponds to the critical exponent of the correlation length for the universality class of the standard percolation transition, as in the case of the diffusion front. Therefore one expects that the exponent given by Eq. (9) will be $\alpha = 3/7 \simeq 0.428$. In fact, by using the MVI interface, Eqs. (1) and (9) have been verified to hold in recent work [18,32]. Indeed, for the case of a model with two control parameters [32] the results are independent of which parameter is used for tuning the percolation transition.

The exponent entering in the scaling law of the number of particles of the MVI (N_{MVI}), as yielded by the GM, is expected to be the same as that for the diffusion front [Eq. (2)], since it is not possible to measure the number of particles in units of the immunity. Then, we have

$$\frac{N_{\mathrm{MVI}}}{L_{\mathrm{y}}} \sim \Delta^{-\alpha^N} \quad \text{where} \quad \alpha^N = \frac{1}{1+\nu}. \tag{10}$$

Again using $\nu = 4/3$, one has $\alpha^N = 3/7 \simeq 0.4286$.

By using the GM one can study not only the percolation transition underlying the model, but also IPTs, as in the case of the irreversible continuous phase transition of the FFMIT. In fact, from the snapshot of Fig. 1(a) one can see that both the active phase (on the left-hand side of the sample) and the absorbing phase (on the right-hand side of the sample) coexist in the same simulation. In order to study IPTs one needs to define another interface, capable of capturing this kind of phase transition, in the same way as the MVI detects the percolation transition.

The interface that captures the active-absorbing transition (no matter the order of the transition) has a very simple definition: It is given by the set of sites $\{x_j, j = 1, \ldots, L_{\mathrm{y}}\}$ belonging to the absorbing green phase that are in contact with the active phase, but are located on the rightmost side of the sample [18]. This interface is a *single-valued interface*, so we call it the SVI.

Figure 1(d) shows the SVI, represented by the dark sites. On the right-hand side of the SVI one has only green trees, defining the absorbing cluster. On the left-hand side of the SVI one has the active phase, but in Fig. 1(d) all states are represented by the same color (for the sake of clarity). Also, Fig. 1(d) shows the mean position of the SVI, represented by the black vertical line.

The average immunity undergone by the sites belonging to the SVI (g^{SVI}) is given by

$$g^{\mathrm{SVI}} = \frac{1}{L_{\mathrm{y}}} \sum_{j=1}^{L_{\mathrm{y}}} g(x_j). \tag{11}$$

Note that the g^{SVI} can be identified with the critical point of the active-absortive transition g_c [18], as in the case of the MVI, where g^{MVI} corresponds to the percolation threshold.

The width of the SVI is given by

$$w^{\mathrm{SVI}} = \sqrt{\frac{1}{L_{\mathrm{y}}} \sum_{j=1}^{L_{\mathrm{y}}} [g(x_j) - g^{\mathrm{SVI}}]^2}. \tag{12}$$

In recent work [18] we have already shown that the SVI also scales according to Eq. (9), for both first- and second-order IPTs. However, now one should consider the suitable exponent that controls the correlation length divergence of the transition in question, as we considered $\nu = 4/3$ for the standard percolation transition. The second-order IPT of the FFMIT belongs to the directed percolation universality class, and the exponent that should be considered in Eq. (9) is $\nu_\perp = 0.733(4)$ [33,34] because it governs the divergence of the correlation length perpendicular to the interface. So, one gets $\alpha^{\mathrm{SVI}} = 0.577$. Also, for both the MVI and the SVI, the exponent α of Eq. (9) governs the convergence of g_p and g_c, respectively, to the critical points.

Summarizing, by using the GM, for both the percolation transition and for the IPTs one has

$$w^x \propto \Delta^{\alpha^x}, \tag{13}$$

$$g_c^x = g_\infty^x + A_x \Delta^{\alpha^x}, \tag{14}$$

$$\alpha^x = \frac{1}{1+\nu_x}, \tag{15}$$

where A_x is a constant and g_∞^x is the extrapolated value of the control parameter at the transition. For the MVI the exponent ν_x is the exponent of the correlation length of standard percolation in $d = 2$ dimensions, $\nu_{\mathrm{MVI}} = \nu = 4/3$, and for the SVI it is the exponent of the correlation length of the directed percolation universality class in $d = 2 + 1$ dimensions, $\nu_{\mathrm{SVI}} = \nu_\perp = 0.733$. These correlation length exponents govern the correlations along the direction perpendicular to the interface, in agreement with the arguments discussed in the context of Eq. (4). Note that for the case of ν_{MVI} one does not need to distinguish between $\nu_\parallel$ and $\nu_\perp$, as in the case of ν_{SVI}, due to the isotropy of the standard percolation cluster.

In Table I we present the expected values for the exponents α^{MVI}, α^{SVI}, and α^N, and the corresponding correlation length exponents that have to be used in Eq. (15). We also quote the universality class of the underlying transition.

Let us also define the absorbing cluster as the cluster composed of all sites on the right-hand side of the SVI, as one can see in Fig. 1(d). On the other hand, the percolating

TABLE I. Expected values for the exponents α^{MVI}, α^{SVI}, and α^{N}, and the corresponding correlation length exponent ν that has to be used in order to evaluate α according to Eq. (15). The last column indicates the universality class of the underlying transition: SP stands for standard percolation and DP stands for directed percolation.

	$\alpha = \frac{1}{1+\nu}$	ν	Universality
α^{MVI}	3/7	4/3	SP
α^{N}	3/7	4/3	SP
α^{SVI}	0.577	0.733	DP

cluster can be seen in Fig. 1(c), and it is composed of sites belonging to the land and the lakes and islands inside the land. The density profiles of these clusters are given by the fraction of the occupied sites for each column $[\rho(x)]$. By using Eq. (5), these profiles can be expressed in terms of the immunity. Henceforth we call these profiles simply the *cluster density* $[\rho(g,\Delta)]$, and we denote the absorbing cluster density by ρ_{abs} and the percolating cluster density by ρ_{perc}.

It is worth noting that from the cluster density $\rho(g,\Delta)$ one can obtain the mean localization of the SVI and MVI (that is, g_c or g_p, respectively), and their fluctuations (that is, the widths w^{SVI} and w^{MVI}, respectively). That function, for finite Δ, varies smoothly within the interval $0 \leqslant \rho(g,\Delta) \leqslant 1$ and tends to the Heaviside step function in the limit $\Delta \to 0$, so that it is not critical at g_c. These properties and the validity of Eqs. (13) and (14) allow us to summarize the expected scaling behavior of ρ, namely (see, for example, Ref. [24])

$$\rho(g,\Delta) = \phi[(g - g_c)/\Delta^{\alpha}], \tag{16}$$

where ϕ is a scaling function. This equation implies that for $g = g_c$ the cluster density should be independent of Δ, and that the curves corresponding to different gradients should cross each other at a fixed point $\rho^* = \rho(g_c,\Delta) = \phi(0)$.

Summing up, we have shown that by using the GM one can obtain the exponent α by measuring w versus Δ [Eq. (13)], and the transition point by determining ρ^*. Furthermore, it can be verified that the scaling ansatz [Eq. (16)] is working out consistently just by collapsing the curves for the cluster density (obtained for different values of Δ) in a single function ϕ, by using the measured values of g_c and α.

Interestingly, we will also show that this kind of analysis, based on Eq. (16), is very general for studying phase transitions. In fact, we have already shown that it is valid for the characterization of first- and second-order IPTs in the Ziff-Gulari-Barshad (ZGB) model [18], and in the present work it is applied to the FFMIT, for both the percolation transition and the second-order IPT.

III. MONTE CARLO SIMULATIONS AND RESULTS

The gradient method was applied to the FFMIT by using lattices with periodic boundary conditions in the vertical direction and open boundary conditions in the horizontal direction, where the gradient of immunity is established, according to Eq. (5). The FFMIT is defined so that each site of a square lattice of size L_x versus L_y can be in one of three states: occupied by a green tree, a burning tree, or empty. Each run starts with a random distribution of trees and empty

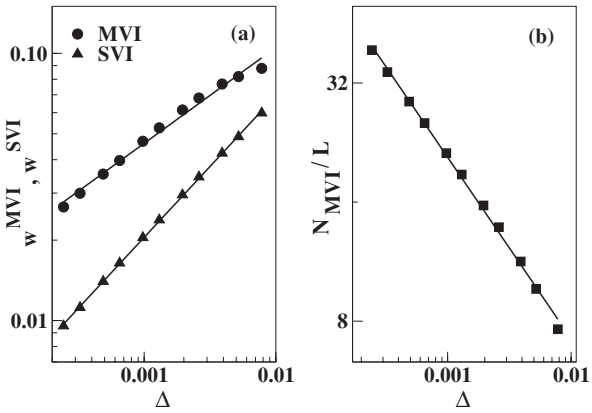

FIG. 2. (a) Log-log plots of w^{MVI} (circles) and w^{SVI} (triangles) as a function of the gradient (Δ), for $p = 0.102$. (b) Log-log plot of N_{MVI}/L (squares) vs the gradient (Δ), as obtained for $p = 0.102$.

sites. During each time step, all sites are updated in parallel, as a cellular automaton, according to the rules defined in the Introduction, with $f = 0$. For the simulations we consider that $L_x = L_y = L$, and we applied a constant gradient $\Delta = 1/L$.

Figure 2(a) shows the log-log plots of the width of both the MVI (w^{MVI}) and the SVI (w^{SVI}) as a function of the gradient (Δ), for $p = 0.102$. These data are consistent with power-law dependences, as expected according to Eq. (13). From a preliminary fit we obtained the exponents $\alpha^{\mathrm{MVI}} \approx 0.3583$ and $\alpha^{\mathrm{SVI}} \approx 0.5305$, both far from the expected values $\alpha^{\mathrm{MVI}} = 0.4286$ and $\alpha^{\mathrm{SVI}} = 0.577$ (see Table I). Figure 2(b) shows the log-log plot of the normalized number of particles belonging to the MVI (N_{MVI}/L) as a function of the gradient (Δ), for $p = 0.102$. From Eq. (10), the linear fit of the data gives $\alpha^{N} \approx 0.4586$, in poor agreement with the expected value $\alpha^{N} = 0.4286$ (see Table I).

However, a careful inspection of Figs. 2(a) and 2(b) reveals a systematic curvature that suggests the occurrence of finite-size effects. In order to overcome this effect we defined L-dependent effective exponents according to

$$\alpha_L^x(L) = \frac{\ln\left(\frac{w^x(L)}{w^x(rL)}\right)}{\ln(r)}, \tag{17}$$

where $x \equiv$ MVI, SVI, and N, and r is a real number.[2] In Fig. 3(a) we show plots of $\alpha_L^{\mathrm{MVI}}(L)$, $\alpha_L^{\mathrm{SVI}}(L)$, and $\alpha_L^{\mathrm{N}}(L)$ versus L, for $p = 0.102$ (we took $r = 2$). The horizontal dashed lines represent the expected values for α^{MVI}, α^{SVI}, and α^{N}. Clearly, the values of the effective exponents $[\alpha_L^x(L)]$ converge to the expected values for $L \to \infty$. Therefore we can use a finite-size correction of the form

$$\alpha_L^x(L) = \alpha^x \pm B_x \left(\frac{1}{L}\right)^{\Phi_x}, \tag{18}$$

where again $x \equiv$ MVI, SVI, and N; while Φ_x are corrections to scaling exponents, and B_x are positive constants. It should be mentioned that the finite-size correction proposed in Eq. (18) has already been used in the measurements of the roughness

[2]If one considers $L_x \neq L_y$, the correct side length to be taken into account in Eq. (17) is L_x.

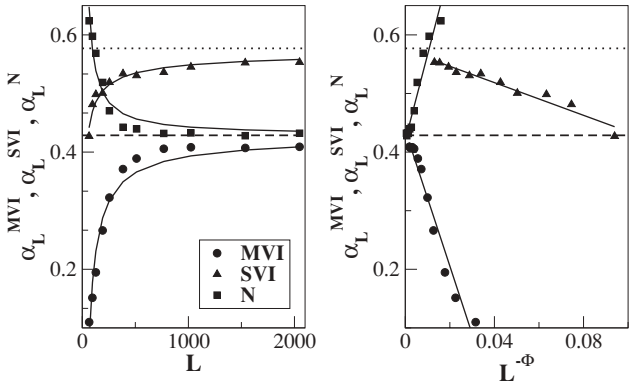

FIG. 3. (a) Plots of $\alpha_L^{\mathrm{MVI}}(L)$ (circles), $\alpha_L^{\mathrm{SVI}}(L)$ (triangles), and $\alpha_L^N(L)$ (squares) vs L, for $p = 0.102$ [data obtained by taking $r = 2$ in Eq. (17)]. The solid lines show the fit of the data obtained by using Eq. (17). (b) Plots of $\alpha_L^{\mathrm{MVI}}(L)$ (circles), $\alpha_L^{\mathrm{SVI}}(L)$ (triangles), and $\alpha_L^N(L)$ (squares) vs $L^{-\Phi_x}$, with $\Phi_{MVI} = 0.8308$, $\Phi_{SVI} = 0.5687$, and $\Phi_N = 0.9945$, as obtained from the fit of Fig. 3(a). For both figures the horizontal long-dashed line represents the exact value for α^{MVI} and α^N, and the horizontal dashed line represents the exact value for α^{SVI} (see Table I).

exponent in the diffusion front [27] and in a ballistic deposition model [35]. From the fit of the data shown in Fig. 3(a) we obtain the values of Φ_x. So, a plot of $\alpha_L^x(L)$ versus $L^{-\Phi_x}$, as shown in Fig. 3(b) for $p = 0.102$, gives us $\alpha^{\mathrm{MVI}} = 0.437(11)$, $\alpha^{\mathrm{SVI}} = 0.574(5)$, and $\alpha^N = 0.420(8)$, all of them in good agreement with the exact values (see Table I).

In Fig. 4 we show plots of α^{MVI}, α^{SVI}, and α^N as calculated for different values of p. Empty symbols represent values obtained with the finite-size correction of Eq. (18) and full symbols represent those obtained without the correction. The excellent agreement with the exact values confirms the validity of the proposed finite-size correction of Eq. (18). The stronger finite-size corrections observed for $p = 0.102$ could be due to

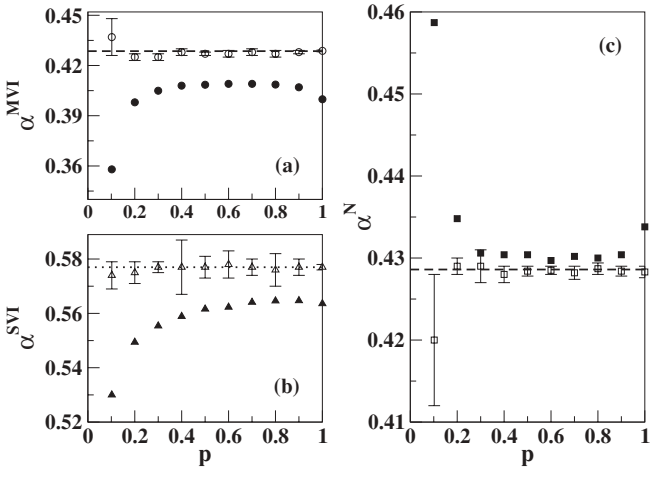

FIG. 4. (a)–(c) Plots of α^{MVI}, α^{SVI}, and α^N, respectively, as calculated for different values of p. Empty symbols correspond to the values obtained by using the correction of Eq. (18), while full symbols correspond to the raw values obtained from fits as shown in Fig. 2. The horizontal lines represent the exact value for α^{MVI} (a), α^{SVI} (b), and α^N (c) (see Table I).

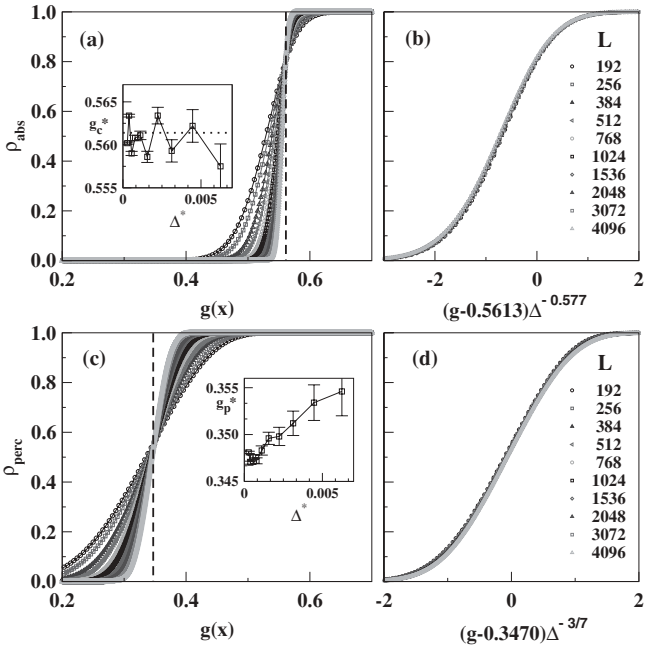

FIG. 5. (a) and (c) show plots of the absorbing cluster density (ρ_{abs}) and the percolating cluster density (ρ_{perc}), respectively, vs $g(x)$, as obtained for samples of different side. The insets of (a) and (c) show the dependence of the intersection point g_c^* and g_p^*, respectively, between curves of consecutive gradients (Δ_1 and Δ_2) with $\Delta^* \equiv (\Delta_1 + \Delta_2)/2$. The extrapolated values of g_c^* and g_p^* obtained by means of a linear fit of the insets were $g_c = 0.5613(8)$ (in excellent agreement with a previous result, $g_c = 0.5614$ [17], shown by the horizontal dashed line) and $g_p = 0.3470(2)$. The vertical dashed lines in (a) and (c) show the extrapolated values of g_c and g_p, respectively. (b) and (d) show scaled plots of the data shown in (a) and (c), respectively. More details in the text.

the closeness to the $p = 0$ point. For this value of p trees cannot grow anymore and the behavior of the model is qualitatively different.

As discussed in Sec. II, by using the gradient method one can also obtain the critical point (g_c) and the percolation threshold (g_p) from the absorbing cluster density (ρ_{abs}) and the percolating cluster density (ρ_{perc}), respectively. In Fig. 5(a) we show ρ_{abs}, whereas in Fig. 5(c) we present ρ_{perc}; both figures were obtained for $p = 0.5$. For the case of ρ_{abs} [Fig. 5(a)] one observes a common intersection point (g_c^*) for all the profiles evaluated for different values of L (i.e., different gradients). A more careful inspection allows us to calculate the intersection points between profiles of consecutive sizes, which extrapolate to the critical point $g_c = 0.5613(8)$, as shown in the inset of Fig. 5(a), in excellent agreement with a previous result, $g_c = 0.5614$ [17]. According to Eq. (16) one can obtain data collapse of ρ_{abs} just by rescaling the horizontal axis by $(g - g_c)\Delta^{-\alpha^{\mathrm{SVI}}}$, as conclusively shown in Fig. 5(b). In the same way, for ρ_{perc} [Fig. 5(c)] the extrapolation of the intersection points tends to the percolation threshold $g_p = 0.3470(2)$. Furthermore, for the percolation transition one can also obtain excellent data collapse of the profiles by scaling the horizontal axis by $(g - g_p)\Delta^{-\alpha^{\mathrm{MVI}}}$ [Fig. 5(d)], as expected from Eq. (16). For different values of p we obtain a similar behavior (not shown here for the sake of space), for

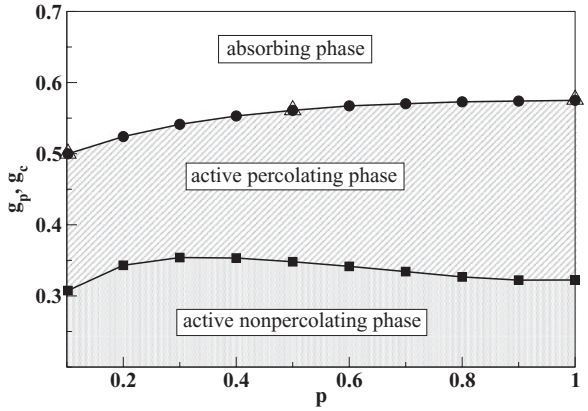

FIG. 6. Phase diagram for the FFMIT as obtained by using the GM. Circles represent the active-absorbing transition (note the excellent agreement with standard results from the epidemic method from Ref. [17], shown as triangles) and squares represent the transition between an active nonpercolating phase and an active percolating phase. More details in the text.

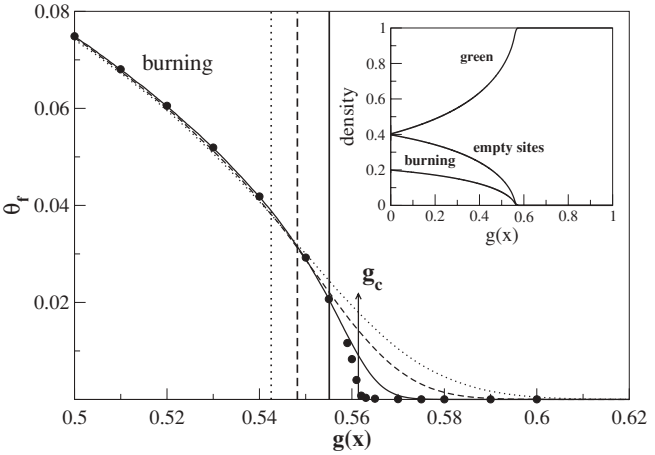

FIG. 7. Comparison of the density of burning trees for the FFMIT calculated according to the standard simulation method (circles) and by using the GM ($L = 512$ dashed line, $L = 1024$ long-dashed line, and $L = 4096$ continuous line), for $p = 0.5$. The critical immunity (g_c) obtained with the GM is indicated by the arrow. The vertical lines correspond to the mean immunity at the location of the SVI ($g^{\rm SVI}$) for the different lattice sides ($L = 512$ dashed line, $L = 1024$ long-dashed line, and $L = 4096$ continuous line). The inset shows the behavior of the density of burning trees, empty sites, and green trees, as obtained by using the GM, for the whole range of immunity ($L = 4096$ and $p = 0.5$).

both the absorbing cluster density and the percolating cluster density.

Alternatively, with the GM one can also obtain the critical points, g_c and g_p, from the mean position of the SVI and the MVI, respectively, by using Eq. (14). In fact, we have recently used that procedure for both the FFMIT and ZGB models [18]. However, the collapse of the cluster density is a more sensitive method to obtain the critical points.

By using the GM, the density of percolating particles at the percolation threshold is obtained from the location of the MVI, as in the case of the diffusion front [19]. For the FFMIT we found that the density of green trees as a function of g [$\theta_{\rm green}(g)$] is independent of the lattice size in the region of the percolation transition. Therefore from the extrapolated value of g_p (obtained previously by the collapse of the cluster density) one obtains the density of green trees at the percolation transition [$\theta_p = \theta_{\rm green}(g_p)$]. For all values of p studied ($0.102 \leqslant p \leqslant 1.0$) we obtained $\theta_p = 0.58(1)$, close to the random percolation threshold ($\theta_c \simeq 0.5927$ [28]).

Figure 6 shows the complete phase diagram for the FFMIT, where besides the usual active-absorbing transition of the model [14,17], we can see a geometrical transition between an active nonpercolating phase and an active percolating phase, as obtained from the GM. The critical line $\{g_c\}$ and the percolating line $\{g_p\}$ shown in the phase diagram, as a function of p, were obtained from the intersection points of both $\rho_{\rm abs}$ and $\rho_{\rm perc}$, as we have already shown for $p = 0.5$ in Figs. 5(a) and 5(c). For the sake of comparison, in Fig. 6 we show the results of the active-absorbing transition obtained by means of the epidemic method ($g_c = 0.5003$ for $p = 0.102$, $g_c = 0.5614$ for $p = 0.5$, and $g_c = 0.5762$ for $p = 1.0$ [17]), all of them in excellent agreement with the results obtained from the GM [$g_c = 0.4997(10)$ for $p = 0.102$, $g_c = 0.5613(8)$ for $p = 0.5$, and $g_c = 0.5752(8)$ for $p = 1.0$].

So far, the results presented here were obtained near the critical points g_c and g_p, which are the intervals where the interfaces SVI and MVI are located. However, we assert that a range of the immunity away from the SVI can also be used in order to gather further important data, usually obtained by using the standard simulation method.

In this way, Fig. 7 shows the density of burning trees for the FFMIT as a function of the immunity g, for $p = 0.5$, as obtained by using the GM (lines) and the standard simulation method often employed to study IPTs (circles). In the case of the standard simulation, each point of the figure corresponds to different simulation runs, whereas for the gradient method the data shown in the figure were obtained in a single simulation (for each lattice size, of course). The vertical lines correspond to the mean immunity of the SVI ($g^{\rm SVI}$) for different lattice sizes, and to the location of the critical point (g_c), as obtained from the GM. From Fig. 7, we observe that for values of g smaller than the location of the SVI ($g < g^{\rm SVI}$), the density of burning trees is independent of the calculation procedure. Of course, $g^{\rm SVI}$ becomes closer to g_c when the gradient decreases, i.e., for larger values of the lattice side L, as expected. The inset of Fig. 7 shows (for $p = 0.5$) the density of burning trees, empty sites, and green trees, as obtained with the GM, and for the whole range of immunity.

Finally, for the region of immunity away from the SVI one can reproduce the results of the standard simulation procedure for the order parameter of the second-order IPT, given by the density of burning trees (θ_f). In fact, for a fixed p, and rather close to the critical point g_c, the order parameter behaves as

$$\theta_f \sim (g_c - g)^{\beta}, \tag{19}$$

where the critical exponent $\beta = 0.583(4)$ corresponds to the directed percolation universality class in $2+1$ dimensions [34].

Figure 8 shows a double-log plot of θ_f versus the deviation of the control parameter $(g_c - g)$ for different gradients. It

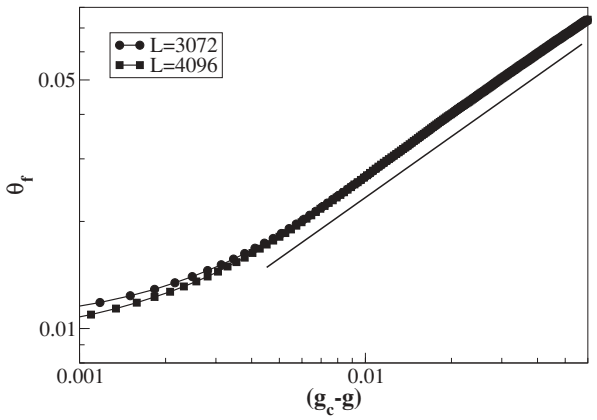

FIG. 8. Log-log plot of the order parameter θ_f for the FFMIT as obtained by using the GM vs the deviation $g_c - g$ of the control parameter ($p = 0.5$). A linear fit gives a slope 0.57(1), which is shown by a full line for the sake of comparison.

is clear that for each gradient there is an interval where the order parameter becomes independent of the gradient. This interval corresponds to values of g smaller than the location of the SVI. By considering the region where size effects are absent ($g < g^{\mathrm{SVI}}$), we can fit a line that gives an estimate of the critical exponent $\beta = 0.57(1)$, in agreement with the expected value. Of course, other stationary values, usually obtained with standard simulations, can also be measured in this interval.

IV. CONCLUSION

We present and discuss the results of a detailed study of the phase transition exhibited by a forest-fire model with immune trees, performed with the aid of the recently proposed "gradient method" for the study of IPTs [18]. By focusing the attention on the interface between the absorptive phase (i.e., the region of the sample fully covered by trees that corresponds to high values of the immunity) and the active phase (i.e., a region where the coexistence of trees, fire, and empty sites is observed for low immunity) one can study the active-absorbing transition of the model. In fact, it is shown that a single-valued interface (SVI) captures the directed percolation behavior characteristics of the second-order IPT of the model. By calculating the SVI one can evaluate the critical immunity and by studying the width of the SVI one can evaluate (after suitable corrections to scaling) the roughness exponent $\alpha^{\mathrm{SVI}} = 1/(1 + \nu_\perp)$, where $\nu_\perp$ is the perpendicular correlation length exponent for the directed percolation (DP) universality class. On the other hand, a multivalued interface (MVI) captures the standard percolation features of the active phase where a percolation transition is observed and characterized. Here, from the MVI one can obtain the critical percolation threshold. Also, for the width of the MVI, as well as for the number of particles of the MVI, one can evaluate (again after suitable corrections) the exponents $\alpha^{\mathrm{MVI}} = \alpha^N = 1/(1 + \nu)$, where ν is the correlation length exponent for the standard percolation universality class. Note that in this case one does not need to distinguish between $\nu_\parallel$ and $\nu_\perp$, as in the case of DP due to the isotropy of the standard percolation cluster. It is worth mentioning that the exponents α^{SVI}, α^{MVI}, and α^N, calculated for the whole range of p ($0.102 \leqslant p \leqslant 1.0$), are in fact independent of p, in agreement with the robustness of the concept of universality. Furthermore, we show that the analysis of the cluster density allows us to locate the critical immunity, not only for the DP transition, but also for the standard percolation transition. We also show that the collapse in a single curve of the cluster density obtained for samples of different side, is a more sensitive method, in order to obtain the critical points, than the mean location of the MVI and SVI, as early proposed [18]. Moreover, these cluster densities can nicely be collapsed by applying simple scaling arguments and by using the determined values of the relevant roughness exponents.

Besides, by means of the GM one can also reproduce the results of the standard simulation procedure. Particulary by analyzing the dependence of the order parameter on the immunity it is possible to evaluate the order parameter critical exponent β, in excellent agreement with the expectations for the DP universality class.

Finally, the gradient method allows us to draw the whole phase diagram of the system, for all range of p, which, besides the usually directed percolation transition, exhibits an additional transition. This transition lies within the active phase that is divided into two subphases: the active percolating and the active nonpercolating ones.

It is worthwhile to mention the interesting work of Caldarelli *et al.* [36] which outlines the relationship between statistical properties of real wildfire spreading and the hull of the percolation cluster of ignited sites, in a percolation model proposed to mimic the dynamics of fire spreading. We think that this challenging topic is of great interest in order to understand the behavior of actual systems in nature, and that within this context the proposed GM would become a powerful tool.

Summing up, by means of numerical simulations and by developing scaling arguments we show that the gradient method is a useful tool for the study of the interplay between standard percolation transitions and IPTs, allowing for their complete characterization. Furthermore, the method allows for the simultaneous study of all the phases involved in a unified fashion and in a single simulation run, which, by the way, is an enormous advantage as compared with standard methods.

ACKNOWLEDGMENTS

We acknowledge financial support from the Argentinian Science Agencies CONICET and ANPCyT, and from the UNLP (Universidad Nacional de La Plata).

[1] E. S. Loscar and E. V. Albano, Rep. Prog. Phys. **66**, 1343 (2003).
[2] A. F. Rozenfeld and E. V. Albano, Phys. Lett. A **332**, 361 (2004).
[3] T. M. Ligget, *Interacting Particle Systems* (Springer-Verlag, New York, 1985).
[4] T. Tomé and J. R. Drugowich de Felício, Phys. Rev. E **53**, 3976 (1996); N. R. S. Ortega, C. F. S. Pinheiro, T. Tomé, and J. R. Drugowich de Felício, Physica A **255**, 189 (1998).

[5] C. P. Ferreira, J. F. Fontanari, and R. M. Zorzenon dos Santos, Phys. Rev. E **64**, 041903 (2001).
[6] N. Guisoni and M. J. de Oliveira, Phys. Rev. E **71**, 061910 (2005); **74**, 061905 (2006).
[7] M. Bär, M. Falcke, H. Levine, and L. S. Tsimring, Phys. Rev. Lett. **84**, 5664 (2000).
[8] S. Coombes and Y. Timofeeva, Phys. Rev. E **68**, 021915 (2003); Y. Timofeeva and S. Coombes, *ibid.* **70**, 062901 (2004).
[9] H. J. Jensen, *Self-Organized Criticality, Emergent Complex Behavior in Physical and Biological Systems* (Cambridge University Press, Cambridge, England, 1998).
[10] P. Bak, K. Chen, and C. Tang, Phys. Lett. A **147**, 297 (1990).
[11] P. Grassberger and H. Kantz, J. Stat. Phys. **63**, 685 (1991).
[12] W. K. Mossner, B. Drossel, and F. Schwabl, Physica A **190**, 205 (1992).
[13] B. Drossel and F. Schwabl, Physica A **204**, 212 (1994).
[14] B. Drossel and F. Schwabl, Physica A **199**, 183 (1993).
[15] S. Clar, B. Drossel, and F. Schwabl, Phys. Rev. E **50**, 1009 (1994).
[16] C. E. Fiore and M. J. de Oliveira, Phys. Rev. E **72**, 046137 (2005); G. P. Saracco and E. V. Albano, J. Chem. Phys. **118**, 4157 (2003).
[17] E. V. Albano, Physica A **216**, 213 (1995).
[18] E. S. Loscar, N. Guisoni, and E. V. Albano, Phys. Rev. E **80**, 051123 (2009).
[19] B. Sapoval, M. Rosso, and J. F. Gouyet, J. Phys. (Paris), Lett. **46**, L149 (1985).
[20] J. F. Gouyet and M. Rosso, Physica A **357**, 86 (2005).
[21] C. I. Addison, J.-P. Hansen, and A. A. Louis, Chem. Phys. Chem.**6**, 1760 (2005).
[22] S. V. Savenko and M. Dijkstra, Phys. Rev. E **70**, 051401 (2004); C. I. Addison, P.-A. Artola, J.-P. Hansen, and A. A. Louis, J. Phys. Chem. B **110**, 3661 (2006); V. A. Ivanov, E. A. An, L. A. Spirin, M. R. Stukan, M. Müller, W. Paul, and K. Binder, Phys. Rev. E **76**, 026702 (2007).
[23] R. F. Voss, J. Phys. A **17**, L373 (1984).
[24] D. Stauffer and A. Aharoni, *Introduction to the Percolation Theory* (Taylor & Francis, London, Washington, DC, 1992).
[25] P. Nolin, Ann. Probab. **36**, 1748 (2008).
[26] A. L. Barabasi and H. E. Stanley, *Fractal Concepts in Surface Growth* (Cambridge University Press, Cambridge, England, 1995).
[27] V. C. Chappa and E. V. Albano, J. Chem. Phys. **121**, 328 (2004).
[28] R. M. Ziff and B. Sapoval, J. Phys. A **19**, L1169 (1986).
[29] M. Kolb, T. Gobron, J.-F. Gouyet, and B. Sapoval, Europhys. Lett. **11**, 601 (1990).
[30] P. Nolin, e-print arXiv:0912.3770v1.
[31] A. Gabrielli, M. A. Muñoz, and B. Sapoval, Phys. Rev. E **64**, 016108 (2001).
[32] M. T. Gastner, B. Oborny, D. K. Zimmermann, and G. Pruessner, Am. Nat. **174**, E23 (2009).
[33] M. Henkel, H. Hinrichsen, and S. Lubeck, *Non-equilibrium Phase Transitions and Critical Phenomena, Volume I. Absorbing Phase Transitions* (Springer, Bristol, UK, 2008).
[34] J. Marro and R. Dickman, *Nonequilibrium Phase Transitions and Critical Phenomena* (Cambridge University Press, Cambridge, England, 1999).
[35] F. D. A. Aarão Reis, Phys. Rev. E **63**, 056116 (2001).
[36] G. Caldarelli, R. Frondoni, A. Gabrielli, M. Montuori, R. Retzlaff, and C. Ricotta, Europhys. Lett. **56**, 510 (2001).